Supplementary Information

A family of macrodomain proteins reverses cellular mono-ADP-ribosylation

Gytis Jankevicius[1,2,7], Markus Hassler[1,3,7], Barbara Golia[1], Vladimir Rybin[3], Martin Zacharias[4], Gyula Timinszky[1] & Andreas G. Ladurner[1–3,5,6]

[1]Butenandt Institute of Physiological Chemistry, University of Munich, Munich, Germany. [2]International Max Planck Research School for Molecular and Cellular Life Sciences, Martinsried, Germany. [3]European Molecular Biology Laboratory, Heidelberg, Germany. [4]Biomolecular Dynamics Unit, Department of Physics, Technical University of Munich, Garching, Germany. [5]Center for Integrated Protein Science Munich. [6]Munich Cluster for Systems Neurology. [7]These authors contributed equally to this work. Correspondence should be addressed to G.T. (gyula.timinszky@med.uni-muenchen.de) or A.G.L. (andreas.ladurner@med.uni-muenchen.de).

Supplementary Figures

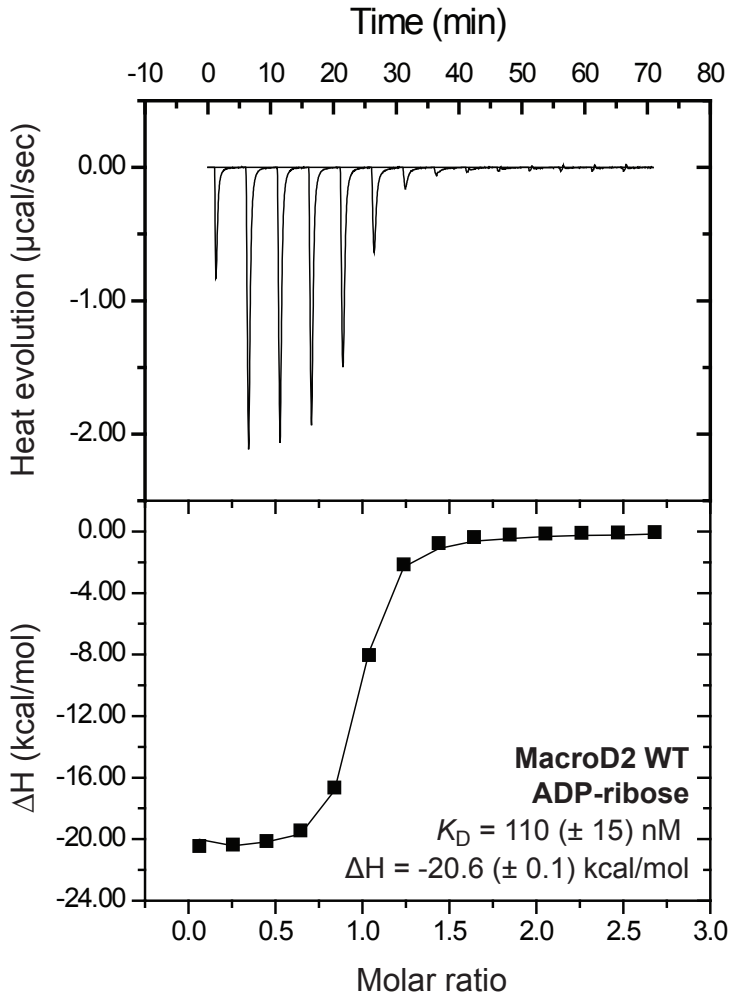

Supplementary Figure 1 | MacroD2 binds ADP-ribose with high affinity. MacroD2 was subjected to isothermal titration calorimetry binding assays with ADP-ribose. Calorimetry profile is depicted at the top. The K_D for ADP-ribose was determined as 110 nM.

Supplementary Figure 2

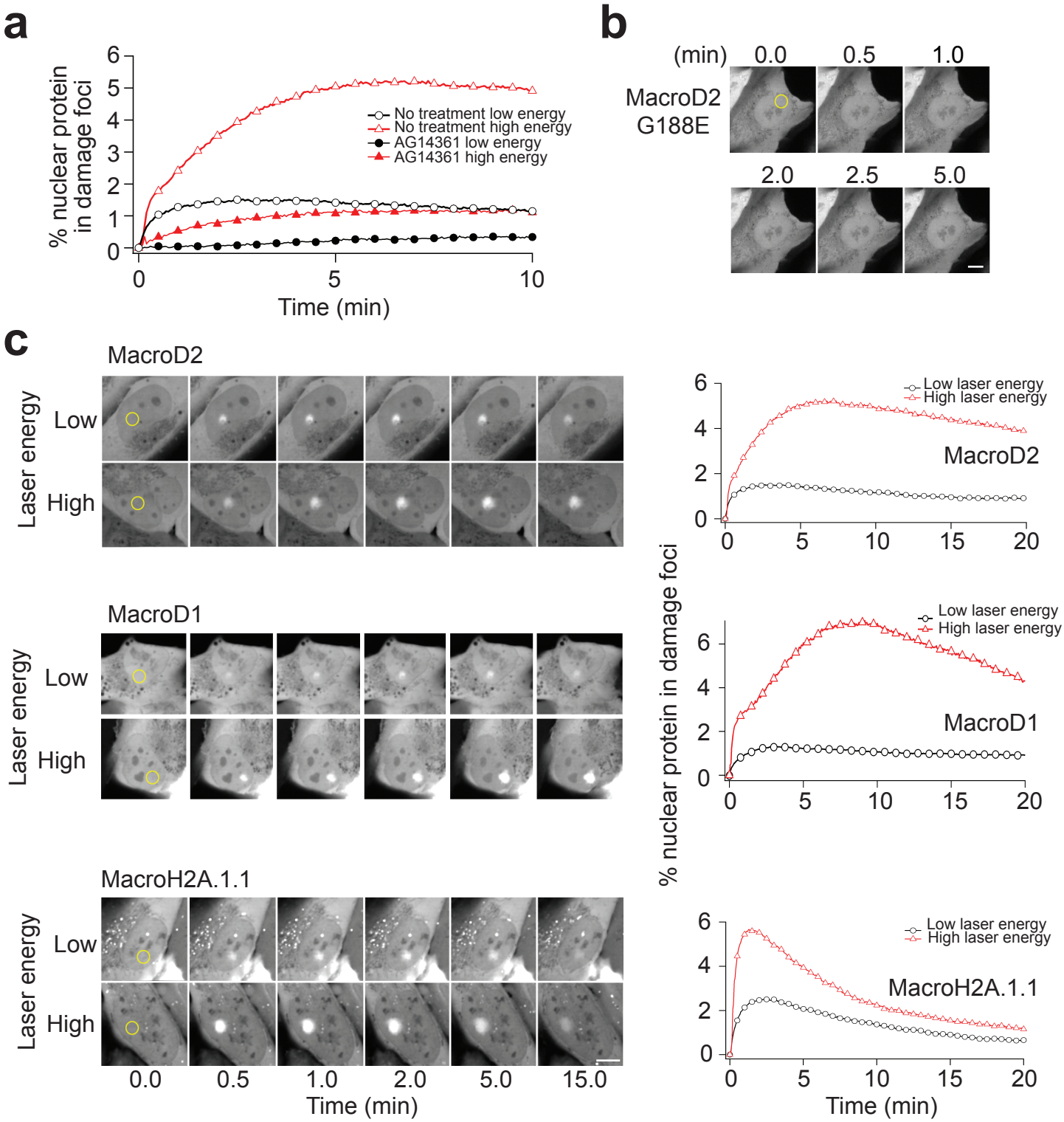

d

Laser energy	N	Time maximum intensity	Value maximum intensity (%)
MacroD2 macrodomain			
Low	5	178 s ± 12	2.8 ± 0.3
High	6	305 s ± 46	4.8 ± 0.6
MacroD1 macrodomain			
Low	>10	186 s ± 17	1.5 ± 0.2
High	>10	471 s ± 42	5.9 ± 0.6
MacroH2A1.1 macrodomain			
Low	6	119 s ± 21	2.0 ± 0.5
High	5	70 s ± 7	5.4 ± 0.5

Supplementary Figure 2 | MacroD2 recruits to DNA damage sites in an ADP-ribosylation-dependent manner but distinctly from MacroH2A.1.1. (**a**) MacroD2 macrodomain recruitment to DNA damage sites depends on ADP-ribosylation. In the presence of the PARP1 inhibitor AG14361 MacroD2 macrodomain recruitment to laser-induced DNA damage is strongly reduced. Representative recruitment profiles shown belong to individual representative cells from each group. (**b**) The ADPr-binding-deficient G188E mutant MacroD2 does not recruit to the site of laser-induced DNA damage. U2OS cells transiently transfected with MacroD2 G188E mutant show no recruitment at the DNA damage site upon microirriadiation at high laser energy. The focus of laser microirradiation is labeled with a yellow circle. Scale bar is 10 µm. (**c**) MacroD2, MacroD1 and MacroH2A.1.1 macrodomains show distinct recruitment profiles. Recruitment of fluorescently-tagged MacroD2, MacroD1 and MacroH2A.1.1 macrodomains to the sites of DNA damage (delimited by a yellow circle) induced with low and high laser power settings. Graphs on the right show representative recruitment profiles of indicated constructs following DNA damage induced with low and high laser power settings. Scale bar is 10 µm. (**d**) Average results for several experiments from c are shown. Mean values with s.e.m. values are represented for the groups of individually analyzed cells.

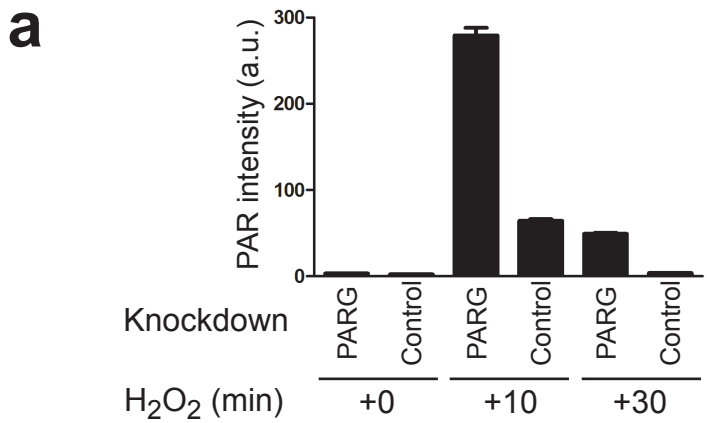

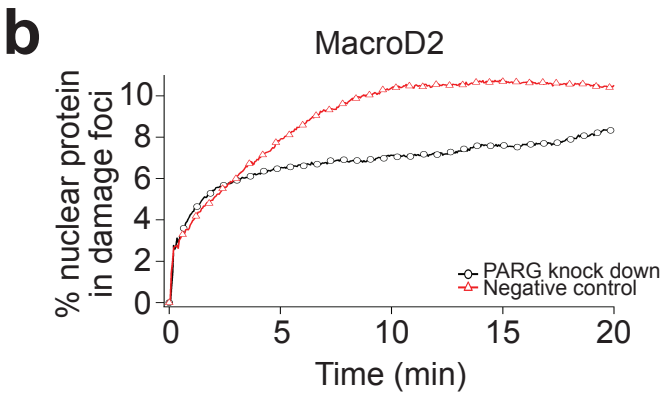

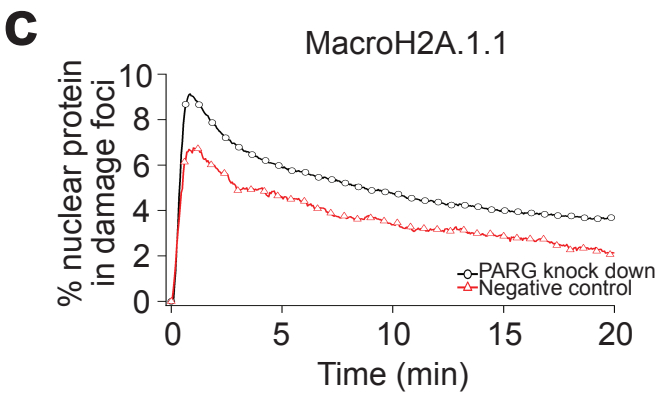

d

Laser energy	N	Time maximum intensity	Value maximum intensity (%)
MacroD2 macrodomain			
PARG knock down			
High	9	1547 s ± 164	6.7 ± 0.4
Negative control			
High	9	919 s ± 112	8.7 ± 0.6
MacroH2A1.1 macrodomain			
PARG knock down			
High	5	76 s ± 1	8.0 ± 0.3
Negative control			
High	4	72 s ± 12	6.8 ± 2.1

Supplementary Figure 3 | PARG depletion changes PARylation levels and MacroD2 recruitment kinetics to DNA lesions. (**a**) PARG knockdown increases H_2O_2-induced PARylation. To test the effects of siRNA-mediated PARG knock-down on PARylation, we treated the cells with 1.2 mM H_2O_2 and fixed them at times indicated following H_2O_2 addition. Poly-ADP-ribose was visualized by anti-PAR (10H) primary and AlexaFluor647-conjugated secondary antibody. PARylation levels were quantified by measuring nuclear AlexaFluor647 fluorescence intensities of individual cells. The graph shows the mean ± s.e.m values. (**b, c**) The recruitment of fluorescently-tagged MacroD2 (**b**) and MacroH2A.1.1 (**c**) macrodomains to sites of laser-induced DNA damage in cells depleted for PARG by siRNA-mediated knock-down. Representative recruitment profiles are shown. (**d**) PARG depletion affects the timing and intensity of MacroD2 recruitment to laser induced DNA lesions. Average results for several experiments from **b** and **c** are shown. Mean values with s.e.m. values are represented for the groups of individually analyzed cells.

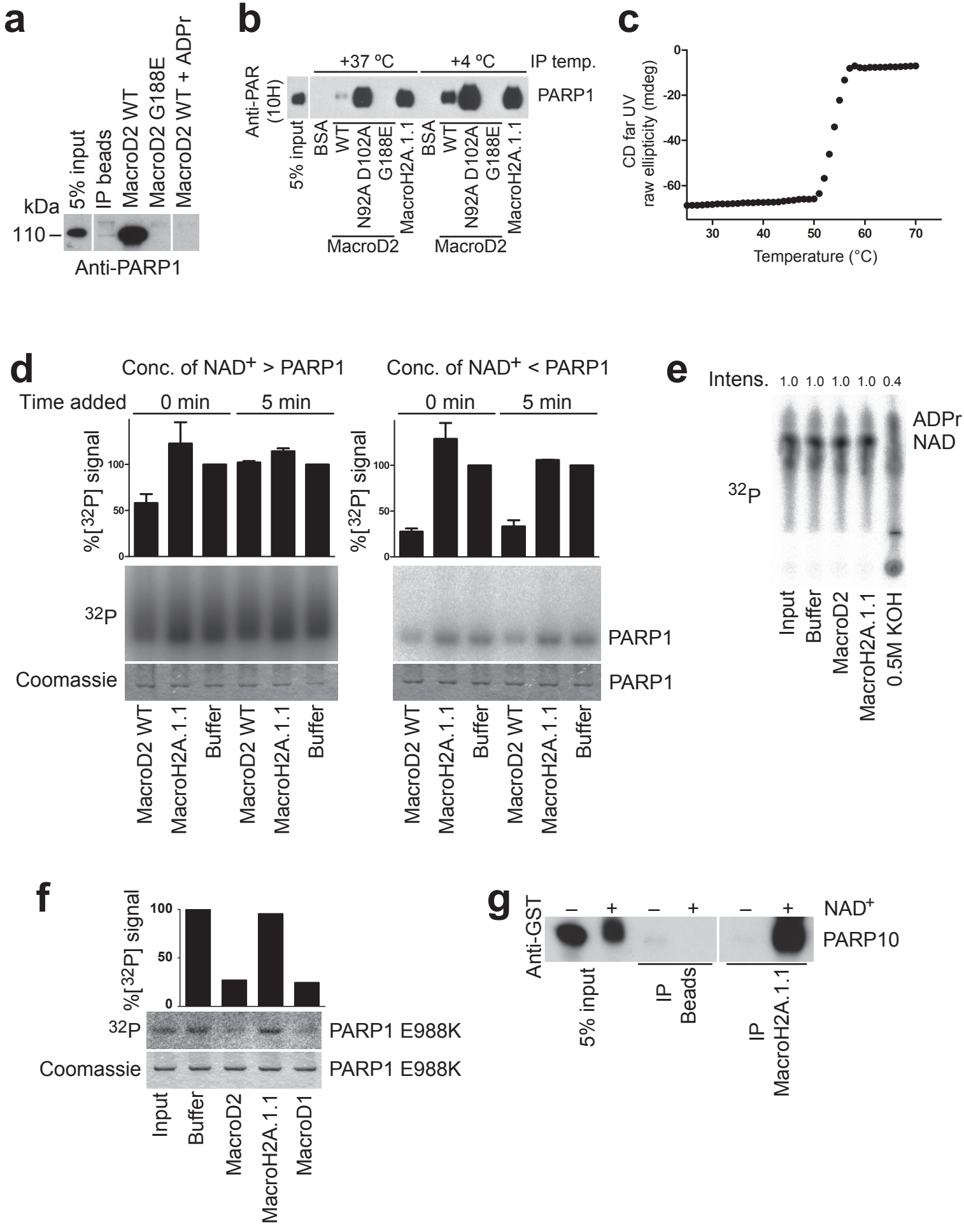
a
kDa
110
5% input
IP beads
MacroD2 WT
MacroD2 G188E
MacroD2 WT + ADPr
Anti-PARP1
b
Anti-PAR (10H)
+37 ºC
+4 ºC
IP temp.
PARP1
5% input
BSA
WT
N92A D102A
G188E
MacroH2A.1.1
MacroD2
c
CD far UV raw ellipticity (mdeg)
Temperature (°C)
d
Conc. of NAD+ > PARP1
Conc. of NAD+ < PARP1
Time added
0 min
5 min
%[32P] signal
32P
Coomassie
PARP1
MacroD2 WT
MacroH2A.1.1
Buffer
e
Intens.
1.0 1.0 1.0 1.0 0.4
ADPr
NAD
32P
Input
Buffer
MacroD2
MacroH2A.1.1
0.5M KOH
f
%[32P] signal
32P
Coomassie
PARP1 E988K
Input
Buffer
MacroD2
MacroH2A.1.1
MacroD1
g
Anti-GST
NAD+
PARP10
5% input
IP Beads
IP MacroH2A.1.1

Supplementary Figure 4 | MacroD2 pulls down PARP1, is folded up to 50 °C and modulates PARP1 activity. (**a**) MacroD2 interacts with PARP1 from HeLa nuclear extracts in an ADP-ribosylation-dependent manner. Immobilized MacroD2 wild-type and ADP-ribose binding-deficient mutant G188E were incubated with HeLa nuclear extracts. To detect PARP1, the pulled-down material was separated by SDS-PAGE and analyzed by Western blot with anti-PARP1 antibody. (**b**) Automodified PARP1 (in the presence of 10 µM NAD^+) was subjected to pulldown experiments with different MacroD2 mutants or MacroH2A.1.1 at 4 or 37 °C. Note the lower pulldown efficiency of MacroD2 at 37 °C compared to 4 °C. Pulled down modified PARP1 was detected by anti-PAR (10H) antibody. (**c**) MacroD2 was subjected to a melting curve experiment by measuring the far UV circular dichroism spectra at different temperatures. The melting temperature (T_m) for MacroD2 is 54.5 °C. (**d**) PARP1 activity is modulated by MacroD2 *in vitro*. PARP1 reactions in the presence of excess or sub-stoichiometric concentrations of NAD^+ were carried out with MacroD2 added prior to, or 5 min after, the start of the PARP1 reaction. The reactions were separated by SDS-PAGE and the autoradiography signal quantified. The error bars represent s.e.m. (n=2). (**e**) [^{32}P]-NAD^+ was incubated under MacroD2 reaction conditions in the presence or absence of macrodomains or 0.5M KOH and separated on TLC plates to assess the stability of NAD^+. After 15 minutes incubation at 37 °C no detectable loss of NAD^+ signal was observed for macrodomain reactions. Relative [^{32}P]-NAD intensity is shown at the top of the TLC plate. (**f**) Both MacroD1 and MacroD2 cleave terminal ADPr from mono-ADPrylated PARP1. PARP1 E988K mutant modified in the presence of [^{32}P]-NAD^+ was subjected to 15 min de-modification reaction at 37 °C by different macrodomain proteins. The samples were separated on polyacrylamide gels and subjected to autoradiography. The removed radioactive signal was quantified and normalized to the buffer control. (**g**) GST-PARP10 catalytic domain was incubated in the absence or presence of NAD^+ and subjected to pull-down by MacroH2A.1.1. GST-PARP10 was detected by anti-GST antibody.

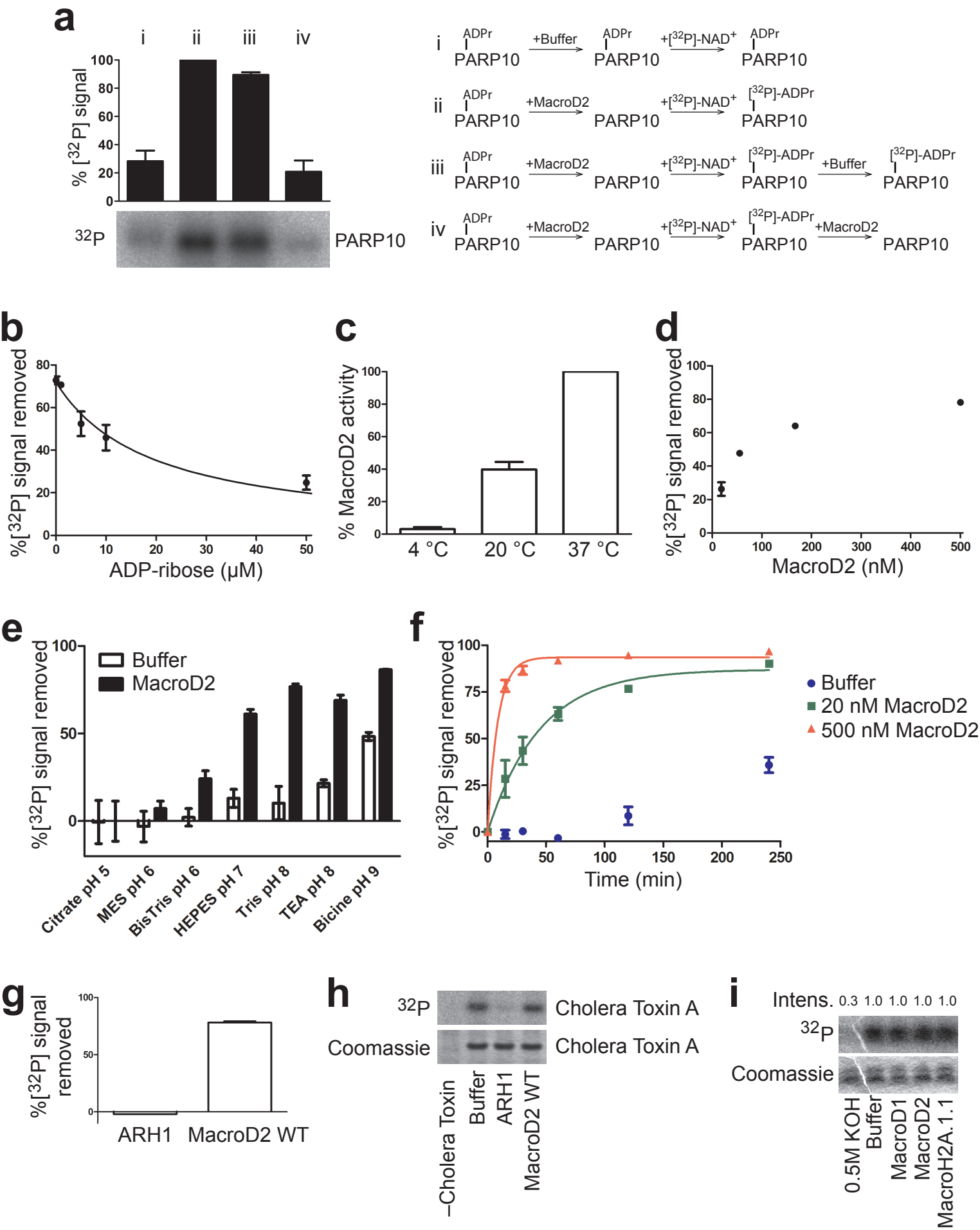
a
i ii iii iv
% [32P] signal
32P
PARP10
i ADPr PARP10 +Buffer ADPr PARP10 +[32P]-NAD+ ADPr PARP10
ii ADPr PARP10 +MacroD2 PARP10 +[32P]-NAD+ [32P]-ADPr PARP10
iii ADPr PARP10 +MacroD2 PARP10 +[32P]-NAD+ [32P]-ADPr PARP10 +Buffer [32P]-ADPr PARP10
iv ADPr PARP10 +MacroD2 PARP10 +[32P]-NAD+ [32P]-ADPr PARP10 +MacroD2 PARP10
b
%[32P] signal removed
ADP-ribose (μM)
c
% MacroD2 activity
4 °C
20 °C
37 °C
d
%[32P] signal removed
MacroD2 (nM)
e
%[32P] signal removed
Buffer
MacroD2
Citrate pH 5
MES pH 6
BisTris pH 6
HEPES pH 7
Tris pH 8
TEA pH 8
Bicine pH 9
f
%[32P] signal removed
Time (min)
Buffer
20 nM MacroD2
500 nM MacroD2
g
%[32P] signal removed
ARH1
MacroD2 WT
h
32P
Coomassie
Cholera Toxin A
Cholera Toxin A
–Cholera Toxin
Buffer
ARH1
MacroD2 WT
i
Intens. 0.3 1.0 1.0 1.0 1.0
32P
Coomassie
0.5M KOH
Buffer
MacroD1
MacroD2
MacroH2A.1.1

Supplementary Figure 5 | **MacroD2 is an enzyme.** (**a**) ADP-ribosylated PARP10 was treated with buffer (reaction i) or MacroD2 (reaction ii) and subjected to a second round of modification in the presence of [^{32}P]-NAD^{+} followed by a treatment with buffer (reaction iii) or MacroD2 (reaction iv). The scheme of the experimental set-up with predicted outcome is depicted on the right. The reactions were separated on polyacrylamide gels and subjected to autoradiography. Radioactive PARP10 signal was quantified and normalized to the pre-modified PARP10 treated with MacroD2 signal (reaction ii). Error bars represent s.e.m. (n=2). (**b-f**) PARP10 demodification reaction by MacroD2 was tested for dependence on (**b**) ADPr product inhibition, line represents a theoretical fit for inhibition; (**c**) temperature; (**d**) MacroD2 enzyme concentration; (**e**) pH; (**f**) incubation time, lines represent a theoretical fit for single turnover kinetics. Demodification reactions with [^{32}P]-ADP-ribosylated PARP10 were carried out by varying the studied parameter, followed by separation on polyacrylamide gels and quantifying the residual [^{32}P]-PARP10 signal on autoradiographs. Where appropriate, the signal was normalized to MacroD2 activity at 37 °C. Error bars represent standard error of the mean (n=2-3). (**g**) ARH1 has no detectable activity towards ADP-ribosylated PARP10. The assay was carried out as in Fig. 3b. (**h**) MacroD2 has no detectable activity towards arginine-linked mono-ADP-ribose. [^{32}P]-ADP-ribosylated Cholera toxin A subunit was subjected to ARH1 or MacroD2 treatment, separated on polyacrylamide gels and subjected to autoradiography. Only ARH1, but not MacroD2, removed ADP-ribose from the Cholera toxin A subunit. (**i**) Neither MacroD1 nor MacroD2 has detectable activity towards lysine-linked mono-ADP-ribose. Non-enzymatically glycated peptide by [^{32}P]-ADP-ribose was subjected to MacroD1, MacroD2 or MacroH2A.1.1 treatment, separated on polyacrylamide gels and subjected to autoradiography. As control, base hydrolysis removes the radioactive [^{32}P]-ADP-ribose signal. No loss of ^{32}P signal upon macrodomain treatment indicates that the ketoamine bond is not hydrolyze by MacroD1/D2.

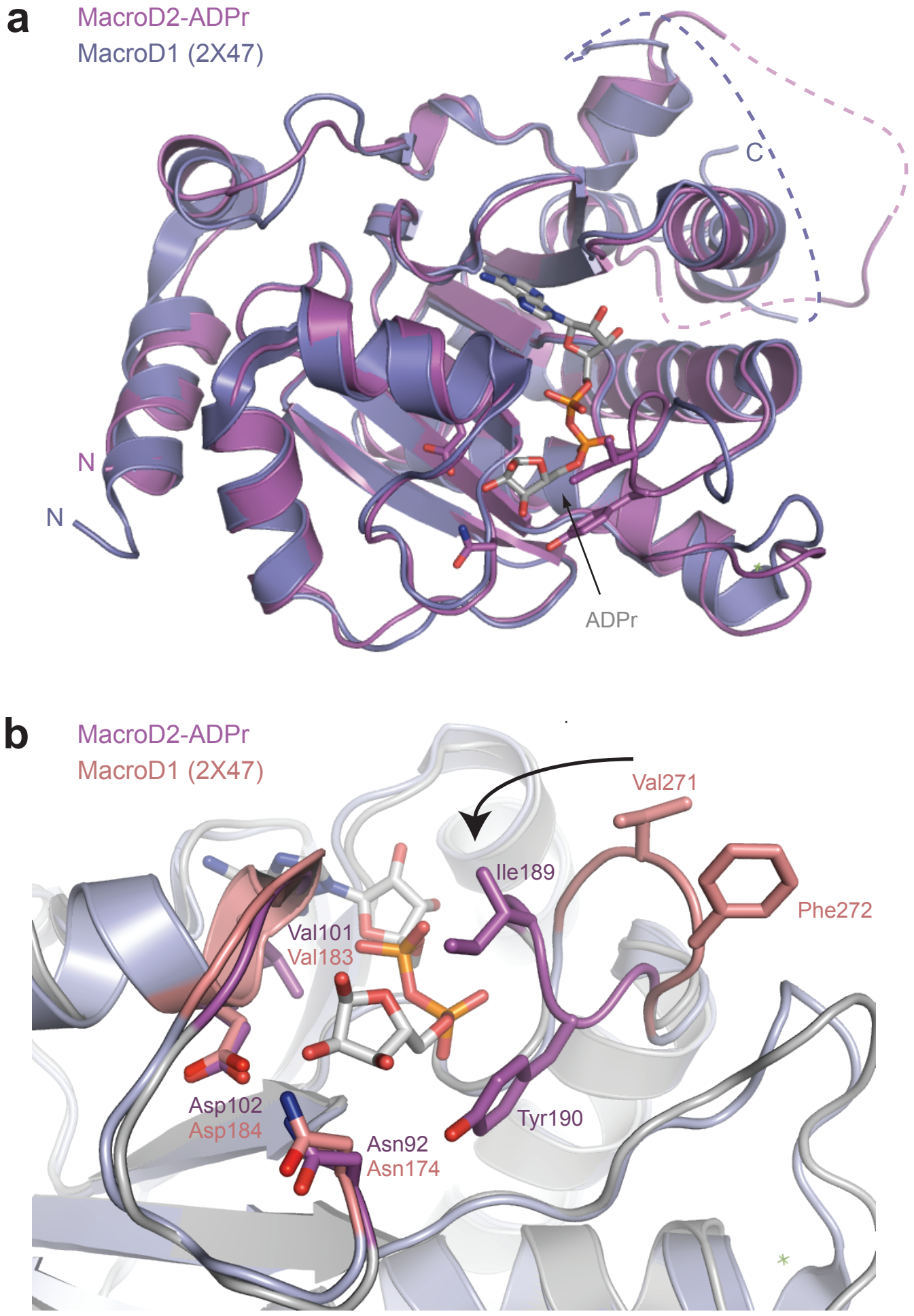
a
MacroD2-ADPr
MacroD1 (2X47)
C
N
N
ADPr
b
MacroD2-ADPr
MacroD1 (2X47)
Val271
Ile189
Phe272
Val101
Val183
Asp102
Asp184
Asn92
Asn174
Tyr190

Supplementary Figure 6 | Superposition of MacroD2-ADPr with MacroD1. (**a**) Overall view of the superposition of human MacroD2-ADPr and human MacroD1 (pdb code 2X47) (rmsd 0.85 Å over 210 Cα atoms). Unstructured loops are indicated by dotted lines. MacroD2 residues forming the distal(Northern) "ribose-binding cleft are indicated in bonds representation. (**b**) Close-up on the distal(Northern) "ribose unit of ADPr (grey). The conformational difference in the ribose-coordinating loop 2 is indicated by a black arrow (13 Å movement between MacroD1 Phe272 and MacroD2 Tyr190).

a

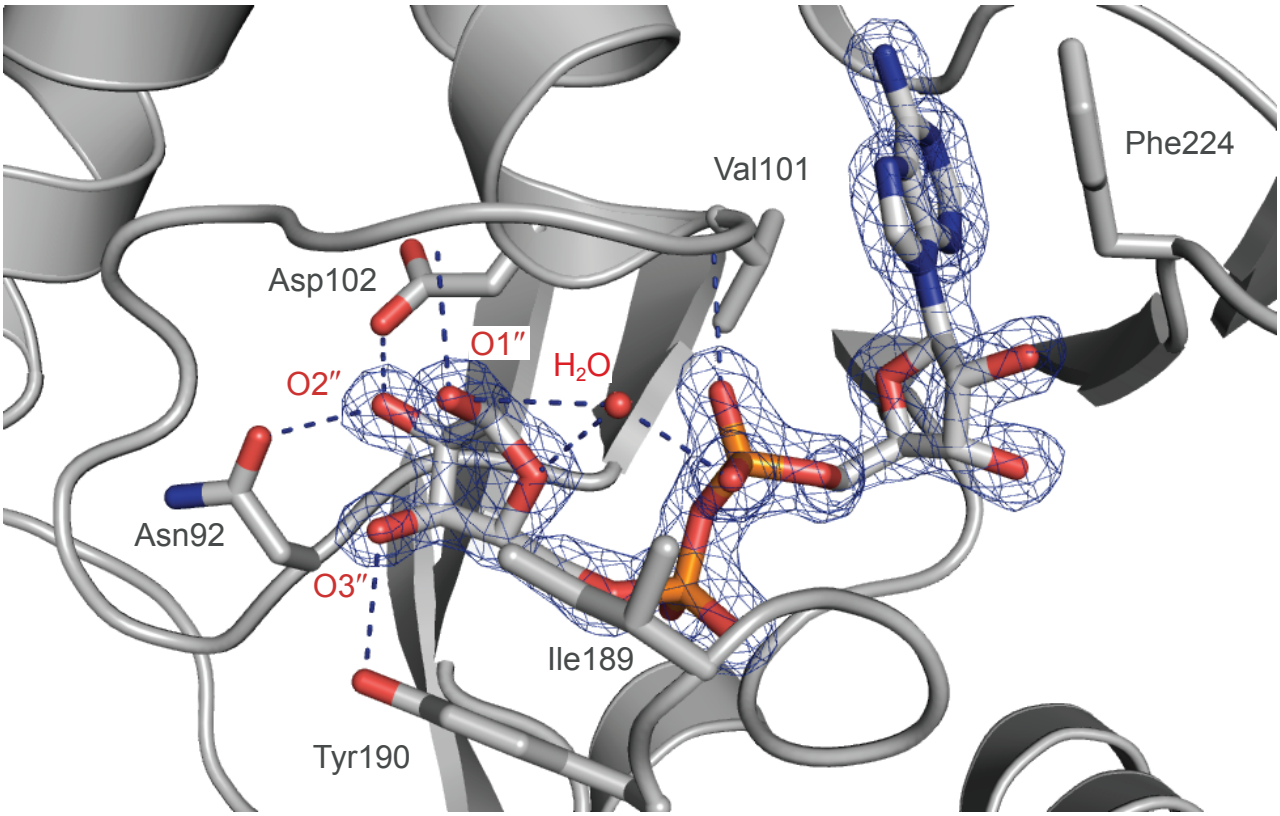
Phe224
Val101
Asp102
O1″
H2O
O2″
Asn92
O3″
Ile189
Tyr190

b

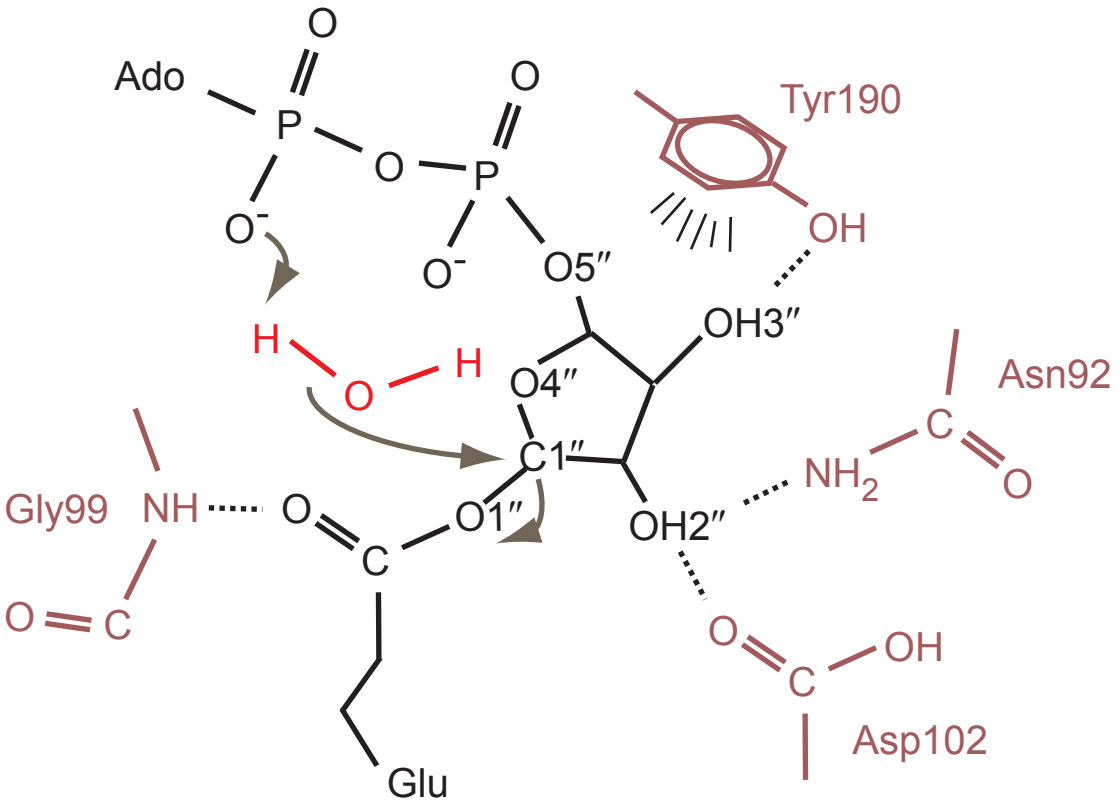
Ado
O
P
O
P
O
O-
O-
O5″
Tyr190
OH
OH3″
H
O
H
O4″
Asn92
C1″
NH2
C
O
Gly99
NH
O
C
O1″
OH2″
O
C
O
C
OH
Glu
Asp102

Supplementary Figure 7 | **MacroD2 ADP-ribose binding pocket and proposed mono-ADP-ribosyl ester hydrolysis catalytic mechanism.** (**a**) Close-up view of the MacroD2 macrodomain in complex with ADPr (in bonds representation) together with a 2|Fo – Fc| electron density map contoured at 1.5 σ (blue). Residues involved in ligand contacts are labeled in grey. The location of OH groups 1-3 of the ''ribose and of the presumed catalytic water molecule are highlighted in red. H-bond contacts involving the ''ribose and the presumed catalytic water are highlighted by dotted lines (blue). (**b**) A proposed mechanism for the hydrolysis of glutamate-linked ADPr. The negatively charged phosphate units of the ADP-ribose render the catalytic water in their vicinity more nucleophilic. The activated water molecule in turn attacks the C1'' electrophile of the distal(Northern) ''ribose, followed by the release of free ADP-ribose and peptide.

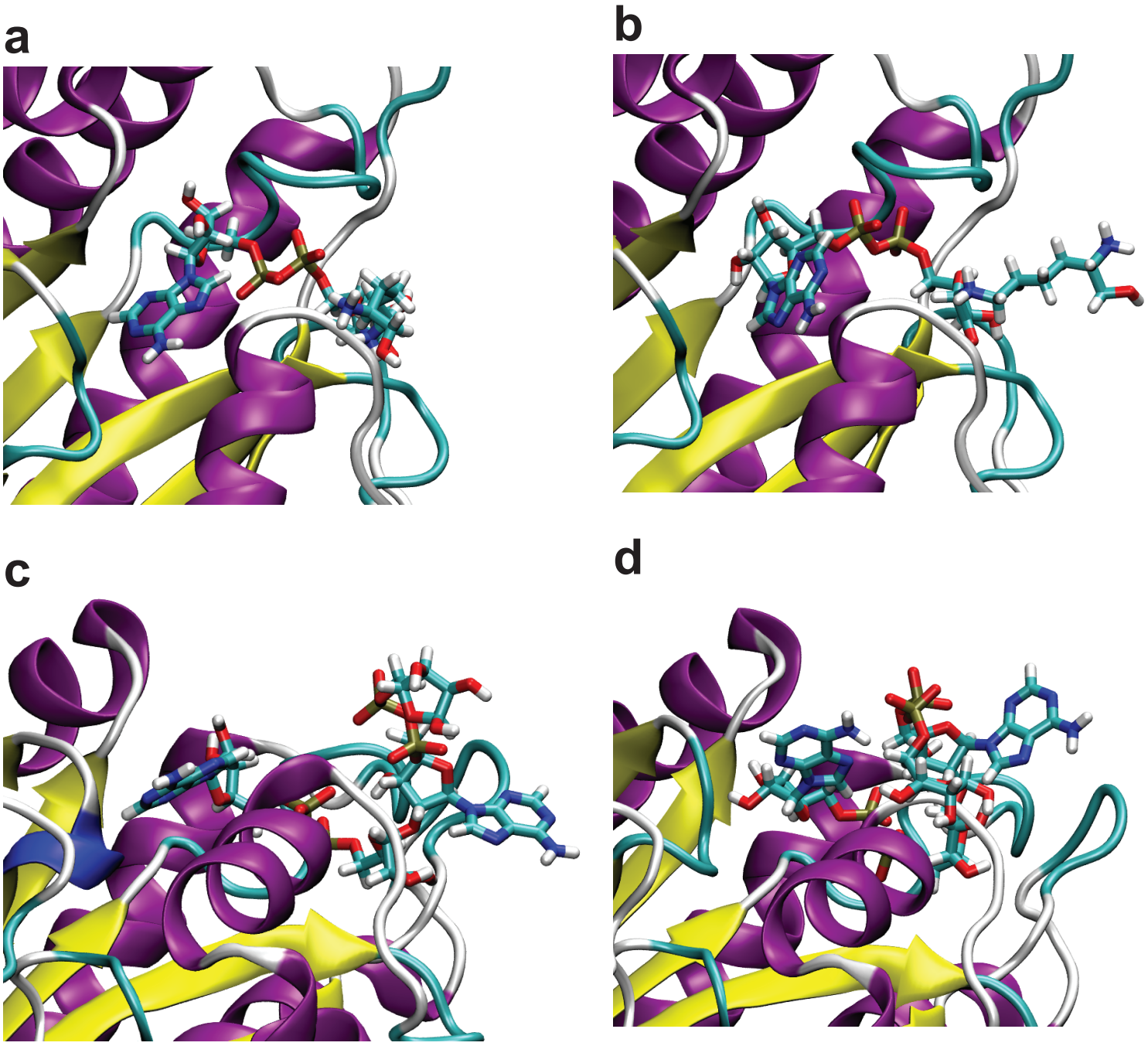

Supplementary Figure 8 | Molecular dynamics (MD) simulations of MacroD2 with Lys-Ketamine-ADPr or di-ADPr. Snapshots from simulations of MacroD2 in complex with Lys-Ketamine-ADPr (**a,b**) and in complex with di-ADPr (**c,d**) are shown. The enzyme is in cartoon representation and the ligands are shown as stick models. The start structures (**a,c**) were obtained by docking the Lys-Ketamine-ADPr and di-ADPr, respectively, in the same placement as in the known MacroD2-ADPr complex structure avoiding any sterical overlap. Residual sterical clashes were removed by energy minimization. MD runs were performed in the same way as described for the ADPr-Glu-ester–MacroD2 complex (see Figure 3c and Methods). Snapshots in the final stage of the simulations (~10 ns) show significant conformational changes of the ligands and partial dissociation (compare panel **d** vs. **c** and **b** vs. **a**).

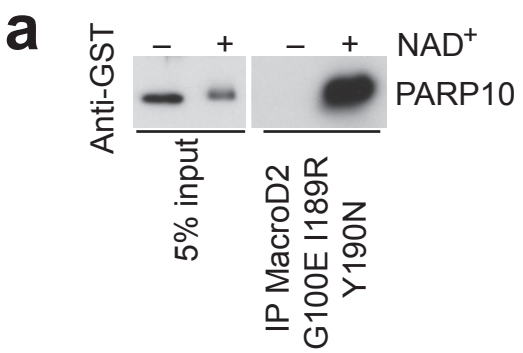

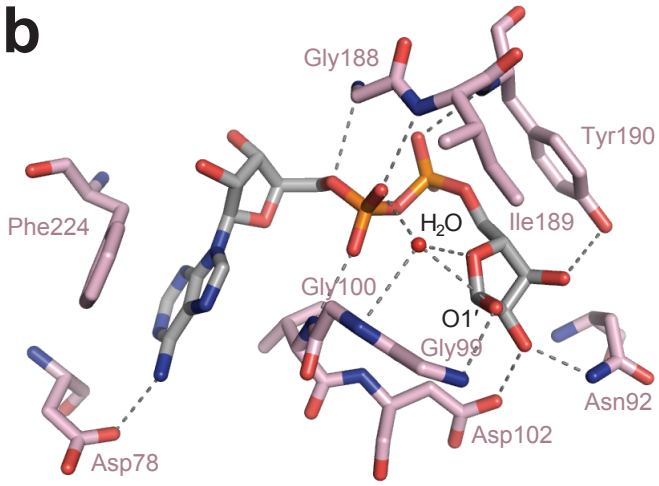

c

MacroD2 mutant	% WT activity	K_D (μM)
WT	100	0.11
I189R	99	30 nM
F224A	89	0.11
G99E	80	0.10
Y190N	72	0.04
D78A	77	2.90
N92A D102A	71	0.93
G100S	65	2.28
G100E I189R Y190N	0	0.55
*G100E Y190N	–23	4.42
*MacroH2A.1.1	–32	1.90
G188E	26	>45
G100E I189R	23	7.36
G100E	12	>113

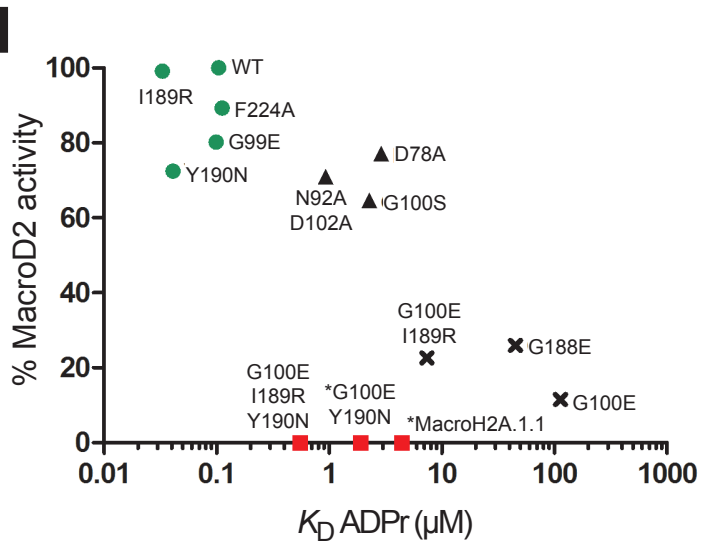

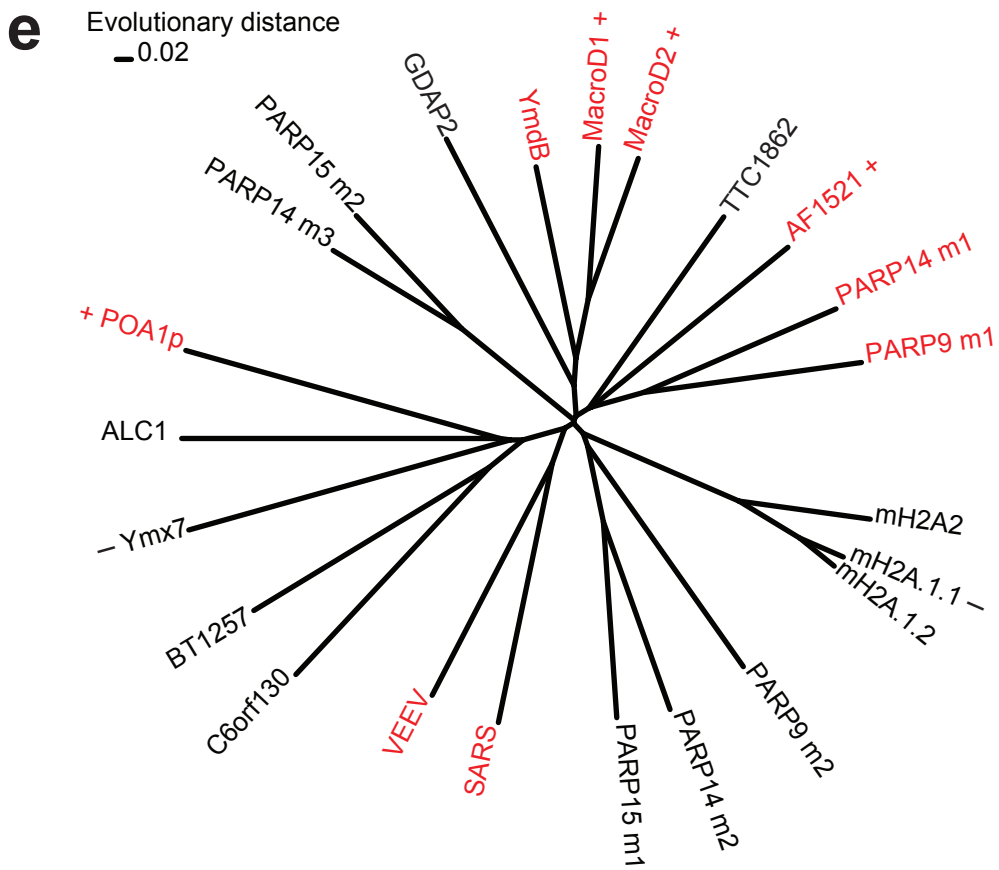

Supplementary Figure 9 | **Validation of the MacroD2 catalytic mechanism and evolutionary conservation.** (**a**) GST-PARP10 catalytic domain was incubated in the absence or presence of NAD^+ and subjected to pull-downs by MacroD2 G100E I189R Y190N mutant. The pulled-down PARP10 was detected by anti-GST antibody. (**b**) ADP-ribose coordination in MacroD2. Close-up view of the ADPr molecule (grey) and amino acid residues (pink) from the binding pocket contacting the ligand and substituted in our mutational analysis (**c,d**) (pink). The catalytic H_2O molecule is shown in red. Protein-ADPr hydrogen bond contacts are highlighted by dotted lines (grey). (**c**) Summary of MacroD2 mutant activities towards ADP-ribosylated PARP10 as normalized to wild-type MacroD2 and ADP-ribose dissociation constants as determined by ITC. The sections divide the mutants into four groups: MacroD2 wild-type-like, intermediate ADP-ribose binders with intermediate ADP-ribosyl-hydrolase activity, MacroH2A.1.1-like, and bad ADP-ribose binders with very low activity. The asterisks indicate that MacroH2A1.1 and MacroD2 G100E Y190N binding seems to protect form non-enzymatic base hydrolysis, probably, by shielding the ester bond from solvent access and result in negative activity if compared to wild type MacroD2 activity. (**d**) [^{32}P]-ADP-ribosylated PARP10 de-modification by MacroD2 mutant activities at 37 °C for 15 min were determined, normalized to the wild-type activity and plotted against the corresponding ADP-ribose dissociation constants as determined by ITC. Green filled circles represent a MacroD2 wild-type-like affinity and activity mutants, triangles - the intermediate ADP-ribose binders with intermediate activity, crosses - the mutants with almost no ADP-ribose binding and very low activity. Red squares mark mutants with MacroH2A.1.1-like ADPr coordination. An asterisk indicates that a negative normalized activity was adjusted to zero. (**e**) The unrooted phylogenetic tree illustrates evolutionary relationships between selected macrodomain proteins. Macrodomain proteins with proposed mono-ADP-ribosyl hydrolysis activity are shown in red. Tested proteins are marked with + for active or – for inactive. The tree includes all human macrodomains (MacroD1, MacroD2, ALC-1, MacroH2A.1.1, MacroH2A.1.2, MacroH2A.2, PARP14 macro 1-3, PARP9 macro 1-2, PARP15 macro 1-2, C60rf130, GDAP2), *E.coli* YmdB, *T. thermophilus* TTC1862, *A. fulgidus* AF1521, SARS Nsp3, VEEV Nsp3, *B. thetaiomicron* BT1257, *S. cerevisiae* Ymx7 and *S. cerevisiae* Poa1p.

Supplementary Note

Molecular dynamics simulations

Molecular dynamics (MD) simulations on MacroD2 in complex with an ADPr-Glu ester model were performed using the Amber11 package[1]. The ADPr-Glu ester was parameterized using the Antechamber module of Amber11 and the ester ligand was docked into the ligand binding site by superposition of the ADPr part on the crystal structure of ADPr in complex with MacroD2. The resulting structure was energy minimized and served as a start structure for MD simulations. The complex was solvated in an octahedral box using the TIP3P water model[2] and neutralized by adding sodium and chloride ions. The system was heated to 300 K employing positional restraints on the solute atoms followed by a stepwise relaxation of the positional restraints. After a 5 ns equilibration simulation without restraints the conformational dynamics and water binding was investigated during 10 ns production at 300 K and a constant pressure of 1 bar.

Structure-guided sequence alignments

Structural superpositions and alignments were calculated using the Indonesia software package[3]. Structural models for yeast Poa1p and ALC-1 were calculated using the PHYRE2 threading server[4].

Pull-downs from HeLa nuclear extracts and PARP1 identification

Nuclear extracts (NE) were prepared essentially as described previously[5], aliquoted, flash frozen in liquid nitrogen and stored at –80 °C. For the pull-downs, NE from ~10^8 nuclei were dialyzed to pull-down buffer (25 mM Tris pH 7.5, 150 mM KCl, 2 mM $MgCl_2$, 0.2 mM EDTA, 0.5 mM DTT and 0.2 mM PMSF). Dialyzed extracts were centrifuged for 10 minutes at 20,000 x g at 4 °C and supernatant incubated for 2 hours at 4 °C in a total volume of 250 µL with MacroD2 proteins immobilized on 10 µL anti-V5 agarose beads, with 17 µM ADP-ribose, where applicable. Beads were washed 4x 1 mL pull-down buffer containing 0.1% NP-40, and boiled in 30 µL gel loading buffer. The samples were separated on 1 mm Bis-Tris, 4–12% acrylamide NuPAGE gel according to the manufacturers protocol (Invitrogen). The gel was stained with Coomassie G-250 and a band at ~110 kDa appearing only in the MacroD2 wild-type protein pull-down was cut out for identification by peptide mass fingerprinting, which was performed by the EMBL Proteomics Core facility. The same pull-down samples were also subjected to immunodetection with anti-PARP1 antibody (1:5000 dilution, rabbit polyclonal, a gift from P. O. Hassa (University of Zurich, Zurich, Switzerland).

***In vitro* PARP1 pull-down assays**

For automodification, 4 ng/µL PARP1 full-length protein was incubated for 15 minutes at 37 °C in the reaction buffer (100 mM Tris pH 7.8, 50 mM NaCl, 10 mM $MgCl_2$, 0.2 mM DTT) containing DNA oligonucleotides and indicated amounts of β-NAD^+. The reactions were then incubated with macrodomain proteins immobilized on 10 µL anti-V5 agarose affinity gel for 1 hour at 4 °C, washed 5 times 1 mL IP buffer (50 mM Tris pH 7.5, 200 mM NaCl, 4 mM $MgCl_2$, 0.1% NP40 and 0.2 mM DTT), boiled in gel loading buffer and separated on NuPAGE gels (Invitrogen), transferred on nitrocellulose membranes and subjected to immunodetection with anti-PAR (10H) ascites.

For co-incubation experiments, MacroD2 (final concentration of 3–4 µM) was added to the PARP1 at different time-points and reactions were allowed to proceed at 37 °C for a total of 15 minutes. After cooling down on ice the pull-downs on MacroD2 were performed as above by adding anti-V5 agarose affinity gel. For temperature dependency of the pull-downs, they were performed as above at either 4 or 37 °C.

PARP1 demodification and *in-vitro* PARP1 activity modulation

For automodification, 10 ng/µL (~90 nM) PARP1 full-length protein was incubated for 15 minutes at 37 °C in the PARP reaction buffer (100 mM Tris pH 7.8, 50 mM NaCl, 10 mM $MgCl_2$, 0.2 mM DTT) containing DNA oligonucleotides and β-NAD^+. PARP1 E988K mutant was used at 20 ng/µL, incubated for 30 minutes with higher [^{32}P]-NAD concentration. For the higher modified PARP1 (molar excess of NAD^+), the final NAD^+ concentration was ~0.625 µM, for low PARP1 modification (substoichiometric NAD^+ concentrations) it was ~15.6 nM, the reaction contained [^{32}P]-NAD (Perkin Elmer). The reaction was stopped by addition of PARP1 inhibitor PJ-34 to a final concentration of 2.5 µM and subjected to 0.45 µM MacroD2, MacroH2A.1.1 or ~1 mU PARG (Enzo Life Sciences) treatment at 37 °C for 15 minutes. The reactions were stopped by gel loading buffer and heating at 95 °C. The samples were separated on NuPAGE gels, gels were dried and exposed to imaging plates (Fuji Film). For autoradiograph quantification, the AIDA 4.0 software package was used.

In vitro activity modulation was checked by performing PARP1 de-modification reactions for a total of 15 minutes (see above), with the exception that 0.5 µM MacroD2 or MacroH2A.1.1 were present during the reaction. The macrodomains were added either before NAD^+ addition or after the PARP1 reaction had proceeded for 5 minutes.

NAD stability was assessed by incubating 2 µM of [^{32}P]-NAD under the PARP demodification reaction conditions in the presence of buffer control, 0.5 µM MacroD2, MacroH2A.1.1 or 0.5M KOH. The samples were separated on silica gel 60 HPTLC plates (Merck) using 1.5 M LiCl with 20% ethanol as eluent and exposed to imaging plates (Fuji Film).

PARP10 pull-downs by macrodomains

GST-PARP10 catalytic domain non-modified or auto-modified (15 minutes reaction in the presence of 1 mM NAD^+) was incubated with V5 tagged macrodomains immobilized on anti-V5 affinity gel for 60 minutes at 4 °C in the IP buffer (50 mM HEPES pH 7.2, 150 mM KCl, 4 mM $MgCl_2$, 0.2 mM DTT and 0.1% NP40). The beads were washed 5x 1 mL with IP buffer, boiled with 25 µL gel loading buffer and separated with SDS-PAGE. The proteins were transferred on nitrocellulose and subjected to immune-detection with anti-GST 1:1000 dilution of in house raised against GST polyclonal antibody.

PARP10 de-ADP-ribosylation reactions

For one de-modification reaction, ~30 pmol GST-PARP10 catalytic domain was bound to 10 µl glutathione sepharose beads for 30 minutes at 4 °C. The beads were washed 3x 1 mL with IP buffer (50 mM HEPES pH 7.2, 150 mM KCl, 4 mM $MgCl_2$, 0.2 mM DTT and 0.1% NP40), and incubated with 0.625 µM [^{32}P]-NAD^+ for 15 minutes at 37 °C. To remove unreacted NAD^+, beads were washed 5x 1 mL IP buffer and incubated with 0.5 µM macrodomains in a total volume of 50 µL for 15 minutes at 37 °C (unless indicated otherwise). The reactions were either separated on silica gel 60 HPTLC plates (Merck) using 1.5 M LiCl with 20% ethanol as eluent, or were stopped by addition of gel loading buffer, boiling at 95 °C followed by separation on NuPAGE gels, drying and exposing to imaging plates (Fuji Film). ADPr inhibition of PARP10 was measured by incubating the demodification reaction in the presence of 0-50 µM ADPr. The data were fitted to the inhibition equation %PARP10 demodified = 100% x ($K_{i,app}$ / ($K_{i,app}$ + c_{ADPr})). The data for PARP10 de-modification by MacroD2 over time was fitted to a single turnover kinetic equation: %PARP10 de-modified = 100% x (F x (1–$e^{(-t*k1)}$)), where F is intensity factor, t is time and k1 is reaction constant.

For re-modification reactions of PARP10, GST-PARP10 was immobilized to beads as above, auto-modified in the presence of 1 mM NAD^+, unreacted NAD^+ was washed off and 0.5 µM MacroD2 added for 15 minutes at 37 °C. Beads were washed again and incubated in the presence of 0.625 µM [^{32}P]-NAD^+ for 10 minutes at 37 °C. The reactions were either stopped here, or washed again and incubated with 0.5 µM MacroD2 for 15 minutes at 37 °C.

For testing GST-tagged macrodomain protein activities, the [^{32}P]-NAD^+ after PARP10 auto-modification reaction was not washed off but immediately followed by demodification reactions containing 0.5 µM GST-macrodomain for 15 minutes at 37 °C.

Ketoamine hydrolysis on peptide with ADP-ribosylated lysine

To generate ADP-ribosylated peptide on lysine residue, 160 µM peptide (PAPAKSAPAPKKGSKK-Biotin) was incubated with 1 mM ADP-ribose derived from NAD and [^{32}P]-NAD hydrolysis in 25 mM Tris pH 8.3 at 37 °C for >7 days[6]. The 80 µM peptide was then incubated with either 0.5 M KOH, buffer

control or 2.5 μM macrodomain proteins at 37 °C for 15 minutes. The samples were boiled with SDS-loading buffer and separated on NuPAGE (Invitrogen) gels using 1xMES running buffer. The gels were dried and exposed to imaging plates (Fuji Film).

De-ADP-ribosylation product identification

For mass spectrometry analysis, GST-PARP10 catalytic domain bound to glutathione sepharose beads was modified in the presence of 1 mM NAD^+, washed 5x 1 mL with IP buffer (50 mM HEPES pH 7.2, 150 mM KCl, 4 mM $MgCl_2$, 0.2 mM DTT) and incubated with 0.16 μM MacroD2 or buffer for 1 hour at 37 °C. The supernatant was adjusted to 0.1% TFA, spotted 1:1 with CHCA matrix (1 mg/mL in 50% acetonitrile with 0.1% TFA) and subjected to MALDI-TOF analysis (Voyager DESTR, Applied Biosystems). The data was analyzed using Data Explorer software (Applied Biosystems).

^{18}O incorporation experiments

^{18}O incorporation experiments were performed as described[7]. ADP-ribosylated GST-PARP10 was bound to beads, washed and incubated for 30 minutes at 30 °C in 50 mM pyridine-formic acid (pH 7.0) buffer containing 66% $H_2{}^{18}O$ with 200 nM MacroD2, alternatively ADP-ribose was incubated under the same buffer conditions to assess the levels of non-enzymatic ^{18}O exchange. The supernatants were diluted 1:10 in 100% methanol and samples analyzed by negative ion electrospray ionization mass spectrometry. The intensities of ADP-ribose or ^{18}O labelled ADP-ribose peaks were calculated and plotted as percent of total ADP-ribose peaks' intensity.

Isothermal titration calorimetry

Isothermal titration binding assays were carried out at 25 °C using either MicroCal VP-ITC or iITC200 instruments (GE Healthcare). Binding reactions were carried out in 25 mM Tris, 100 mM NaCl buffer (pH 7.5), using 15–30 μM macrodomains and ADP ribose as a ligand (Sigma). The ligand in the injection syringe was at 10–15 times higher concentration (250–350 μM) than the macrodomains. Data analysis was conducted using Origin software (OriginLab, USA).

Supplementary Note References

1 Case, D. A., D. A. Pearlman, J. W. Caldwell, T. E. Cheatham III, W. S. Ross, C. L. Simmerling, T. A. Darden, K. M. Merz, R. V. Stanton, A. L. Cheng, J. J. Vincent, M. Crowley, V. Tsui, R. J. Radmer, Y. Duan, J. Pitera, I. Massova, G. L. Seibel, U. C. Singh, P. K. Weiner, and P. A. Kollman. Amber 8. *University of California, San Francisco* (2003).

2 Jorgensen, W. L., Chandrasekhar, J., Madura, J. D., Impey, R. W. & Klein, M. L. Comparison of simple potential functions for simulating liquid water. *The Journal of Chemical Physics* **79**, 926-935 (1983).

3 D. Madsen, P. J., and G. J. Kleywegt. Indonesia: An integrated sequence analysis system. (2002).

4 Kelley, L. A. & Sternberg, M. J. Protein structure prediction on the Web: a case study using the Phyre server. *Nature protocols* **4**, 363-371, doi:10.1038/nprot.2009.2 (2009).

5 Dignam, J. D., Lebovitz, R. M. & Roeder, R. G. Accurate transcription initiation by RNA polymerase II in a soluble extract from isolated mammalian nuclei. *Nucleic Acids Res* **11**, 1475-1489 (1983).

6 Fedorova, M., Frolov, A. & Hoffmann, R. Fragmentation behavior of Amadori-peptides obtained by non-enzymatic glycosylation of lysine residues with ADP-ribose in tandem mass spectrometry. *Journal of Mass Spectrometry* **45**, 664-669, doi:10.1002/jms.1758 (2010).

7 Kasamatsu, A. *et al.* Hydrolysis of O-Acetyl-ADP-ribose Isomers by ADP-ribosylhydrolase 3. *Journal of Biological Chemistry* **286**, 21110-21117, doi:10.1074/jbc.M111.237636 (2011).